Sensors and Materials, Vol. 38, No. 11 (2026) 6495–6516
MYU Tokyo

S & M 4692

Optimal Port Virtual Power Plant Scheduling Considering Flexible Shore Power Allocation and Emission Reduction Potential Ranking

Boying Liu,[1,2] Jiaming Wang,[1,2] Hsiung-Cheng Lin,[3*] and Lingling Li[1,2]

[1]State Key Laboratory of Intelligent Power Distribution Equipment and System, Hebei University of Technology, Tianjin 300401, China
[2]Key Laboratory of Electromagnetic Field and Electrical Apparatus Reliability of Hebei Province, Hebei University of Technology, Tianjin 300401, China
[3]Department of Electronic Engineering, National Chin-Yi University of Technology, Taichung 41170, Taiwan

(Received April 25, 2026; accepted July 17, 2026)

Keywords: wind and solar sensors, flexible shore power allocation, port virtual power plant, Stackelberg game

Shore power is considered to play a critical role in reducing carbon emissions from berthed vessels to meet the global shipping industry's decarburization agenda and the International Maritime Organization 2050 net zero emission goal. However, conventional shore power allocation schemes are still unable to appropriately accommodate the power demanded by vessels or the economic conflict arising between the port energy operator and the hierarchical decision-making structure. To meet these challenges, in this study, we propose an optimal scheduling strategy for a port virtual power plant based on flexible shore power allocation and emission reduction potential ranking. High-response-speed ultrasonic wind and solid-state shortwave radiation sensors are deployed to collect key environmental data such as wind speed, wind direction, and solar irradiance at the port area, thereby providing accurate inputs for renewable energy output forecasting. First, a Stackelberg leader–follower game framework is formulated, with the port energy service operator (PESO) acting as the leader and the port-integrated energy system (PIES) as the follower, guiding the optimal dispatch of multiple energy resources through dynamic pricing signals. Second, a shore power priority allocation mechanism based on the dual attributes of vessel emission reduction potential and berthing time window is developed to optimize switching operation between shore a power supply and an onboard generator. Compared with the conventional strategy, the daily operating cost of PIES is reduced by 14.85%, whilst PESO obtains a net profit. The total carbon emission reduces CO_2 to up to 459.35 tons, and the shore power service satisfaction rate improves from 77.18 to 88.30%.

1. Introduction

With the acceleration of the global shipping industry's decarburization process, the International Maritime Organization has explicitly stated the goal to achieve net zero emissions

*Corresponding author: e-mail: hclin@ncut.edu.tw
https://doi.org/10.18494/SAM6384

ISSN 0914-4935 © MYU K.K.

by around 2050.[1] Against this backdrop, shore power technology is regarded as a critical pathway for replacing onboard auxiliary engines to achieve zero emissions at berth ports. The widespread adoption of shore power has profoundly reshaped the interaction between ports and vessels; however, it has also imposed substantial distribution capacity pressure on port power grids.[2,3] To address this challenge, the port-integrated energy system (PIES) and virtual power plan tarchitecture have been proposed, with the objective of enhancing system operational flexibility through the efficient management of multiple energy flows, including electricity, heating, and cooling.[4]

The rapid advancement of sensor technology has provided new impetus for the refined planning and real-time scheduling of port wind, photovoltaic, and storage systems.[5] In complex and variable marine environments, ultrasonic wind sensors and high-stability pyranometers have significantly improved the dimensionality of data acquisition, achieving notable breakthroughs particularly in resistance to salt spray corrosion and dynamic response speed.[6] These advances in sensing technology enable port energy management systems to collect multi-dimensional, high-resolution physical operational data, thereby providing a data foundation for further exploitation of the regulation potential inherent in the flexible shore power loads of vessels.

Shore power loads are not simply static electricity demands; rather, they exhibit pronounced time-varying characteristics and instantaneous high power features.[7] Conventional vessel berthing scheduling predominantly adheres to the first-come-first-served (FCFS) principle. As noted by Imai *et al.*[8] whilst FCFS is straightforward to implement, it often causes inefficient resource allocation during berth congestion and is further constrained owing to high costs and limited connection points.[9] Recent studies have begun to move beyond the limitations of FCFS. Although Wang and Zou[10] explored a coordinated allocation based on vessel types, the refined ranking of vessels by both the emission reduction potential and the berthing time window remains insufficiently addressed in the existing literature.

Existing research on PIESs has begun to evolve from single electricity dispatch towards the coupling of multiple energy flows encompassing electricity, heating, and cooling.[11] Nevertheless, current studies still tend to treat the port as a homogeneous entity or a single microgrid node. For instance, Li *et al.*[12] in their green port cost model considered the coordination of shore power and energy storage, but they did not delineate the substantial differences in physical constraints across functionally distinct terminals. Iris and Lam[13] pointed out that existing models fail to refine the capacity and constraints of areas such as quayside and stacking yards, rendering them inadequate for characterizing instantaneous high-power fluctuations. Although Xiong *et al.*[14] addressed resource heterogeneity, it was mainly focused on generic loads. Sarantakos *et al.*[15] unveiled that, owing to the absence of the detailed modeling of factors such as the number of shore power installations, conventional scheduling strategies prove overly idealized under resource competition scenarios.

Balancing the interests of the operator and vessel users posted another significant issue in the system operation.[16–18] Traditional centralized optimization approaches are difficult to implement in practice because they disregard the decision-making autonomy of individual entities. Wen *et al.*[17] and Zhao *et al.*[19] revealed that, in the absence of a suitable game theoretic

framework, the system cannot reflect user sensitivity to price, thereby limiting the resource response potential. Accordingly, the Stackelberg leader–follower game attracted considerable attention owing to its capacity to characterize multi-level decision-making logic. For example, Pan *et al.*[20] employed price signals to guide behavior, achieving a 42.2% increase in the purchase of shore power by vessels. Sun *et al.*[21] proposed a two-stage framework that realized a win–win outcome for multiple parties through dynamic pricing. However, the deep coupling of dynamic pricing signals with underlying heterogeneous shore power allocation and multiple energy conversions remains a gap in the current literature.

In this study, an optimal scheduling model for a port virtual power plant is constructed considering flexible shore power allocation and emission reduction potential ranking. The model aims to optimize the coordinated operation of multiple energy systems comprising electricity, heating, and cooling under multiple-region heterogeneous constraints. It introduces a resource priority ranking mechanism based on vessel emission reduction potential and berthing time window. Furthermore, a deep coupling of dynamic pricing and flexible resource allocation is achieved through the Stackelberg leader–follower framework. The remainder of this paper is organized as follows. In Sect. 2, we present the framework of the proposed problem. In Sect. 3, we provide the detailed mathematical formulations. In Sect. 4, we demonstrate the effectiveness of the model through a case study. In Sect. 5, we conclude the key contribution and limitation in this study. Future work is suggested for further investigation and development in this area.

2. Problem Description

With the deep decarburization of the shipping industry, seaports are evolving into virtual power plants that integrate multiple energy flows and exhibit substantial regulation capabilities. As illustrated in Fig. 1, the PIES constructed in this study is introduced to support zero emissions at berth through multiple energy coordination.

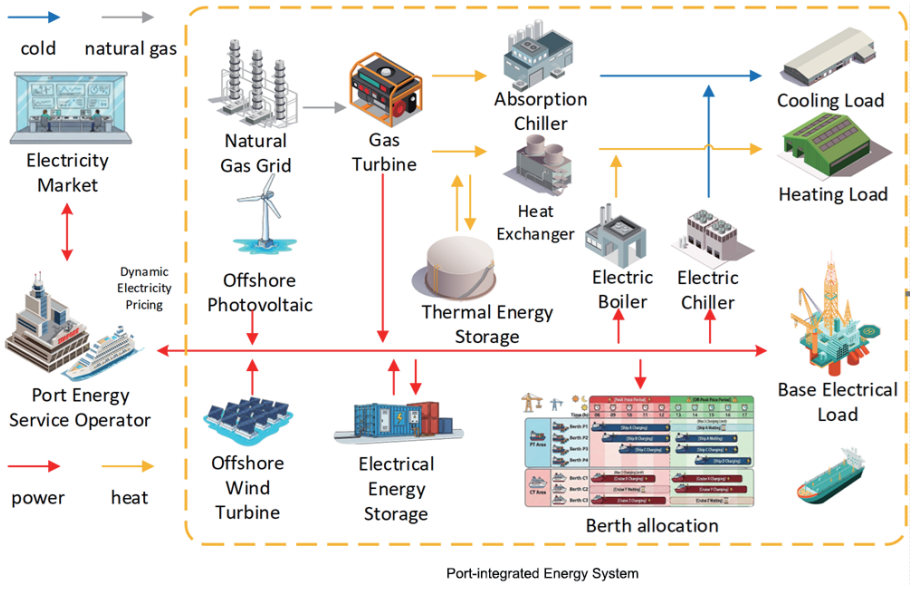

Fig. 1. (Color online) Operational framework of the port virtual power plant.

On the supply side, PIES integrates large-scale offshore wind power (OWT) and photovoltaic power (OPV). To enable accurate forecasting and real-time scheduling, high-response-speed wind, wind direction, and irradiance sensors are deployed on wind turbine blades and photovoltaic arrays for the continuous monitoring of environmental meteorological parameters. The core conversion unit, a gas turbine (GT), achieves combined cooling, heating, and power generation via a heat exchanger (HX) and an absorption chiller (AC). This is supplemented by an electric boiler (EB), an electric chiller (EC), and energy storage systems, including electrical energy storage (EES) and thermal energy storage (TES), to mitigate fluctuations. Within this architecture, the port energy service operator (PESO) acts as the leader, formulating dynamic price signals based on real-time output data aggregated from sensors and external electricity market prices. PIES, as the follower, responds through internal unit optimization and shore power load feedback. This Stackelberg leader–follower game framework enables the coordinated optimization of operator profit and operational cost.

In view of the heterogeneous characteristics of different terminal zones, shore power is regarded as a flexible demand response resource. The system performs dynamic priority ranking on the basis of vessel-reported berthing parameters and emission reduction contributions. Under the constraints of energy balance and supply reliability, the objective is to maximize PESO profit whilst minimizing PIES cost. Detailed mathematical formulations are presented in Sect. 3.

3. Proposed Models

3.1 Mathematical modeling of PIES

3.1.1 Renewable energy generation modeling

The power output of offshore wind turbines is primarily affected by cut-in and cut-out wind speeds.[22] Wind speed is measured in real time by a Gill Windsonic ultrasonic wind sensor mounted on the wind turbine tower at the hub height. Regarding the spatial layout, these high-precision sensors are systematically deployed at key operational nodes across the wind turbine towers and photovoltaic arrays to capture localized meteorological profiles. To ensure forecasting stability, the sensor operates at a high sampling frequencyof 1 Hz , and the raw data is aggregated into 15-min average intervals to serve as the input matrix for the short-term renewable energy forecasting model. These 15-min high-resolution forecasts are subsequently averaged into 1-h block data to strictly align with the discrete time step of PIES's scheduling model. This sensor offers high response speed and robust resistance to salt spray corrosion, rendering it suitable for offshore environments. On the basis of the typical power curve of the wind turbine, the output power model is expressed as

$$P_t^{OWT} = \begin{cases} 0, & 0 \le v_t^{OWT} < v^{in} \\ P^{OWT,r} \cdot \dfrac{v_t^{OWT} - v^{in}}{v^r - v^{in}}, & v^{in} \le v_t^{OWT} < v^r \\ P^{OWT,r}, & v^r \le v_t^{OWT} < v^{out} \\ 0, & v_t^{OWT} \ge v^{out} \end{cases} \tag{1}$$

where P_t^{OWT} is the actual OWT power at time t, $P^{OWT,r}$ is the rated power under standard conditions, v_t^{OWT} is the actual wind speed at time t, and v^{in}, v^r, and v^{out} denote the cut-in, rated, and cut-out wind speeds, respectively.

The actual power output of offshore photovoltaic units is mainly affected by ambient temperature and solar irradiance.[23] Solar irradiance within the system is measured by an Apogee SP-110 self-powered shortwave radiation sensor, which utilizes a solid-state encapsulated design for the stable, long-term measurement of total shortwave radiation in outdoor environments. The output power model is defined as

$$P_t^{OPV} = P^{STC} \cdot \frac{G_t}{G^{STC}} \cdot \left[1 + \gamma^{OPV}\left(T^c - T^{STC}\right)\right] \cdot \eta^{sys}, \tag{2}$$

where P_t^{OPV} is the OPV power at time t, P^{STC} is the rated power under standard test conditions, G_t is the actual total irradiance received at sea, G^{STC} is the vertical irradiance under standard test conditions, γ^{OPV} is the power-temperature coefficient, T^c is the actual operating temperature of the PV cells, T^{STC} is the reference temperature under standard conditions, and η^{sys} is the comprehensive system efficiency.

3.1.2 Energy conversion equipment modeling

The GT produces both electrical and thermal energies simultaneously. Its model is formulated as

$$\begin{cases} P_t^{GT} = \eta^{gas} \cdot F_t^{GT} \cdot LHV^{gas}, \\ H_t^{GT} = P_t^{GT} \cdot \dfrac{1 - \eta^{ge} - \eta^{loss}}{\eta^{ge}}, \end{cases} \tag{3}$$

where η^{gas} is the power generation efficiency of the GT, P_t^{GT} is the electrical power output, and H_t^{GT} is the thermal power output of the GT at time t. System carbon emissions are generated by the GT, grid power purchases, and ship diesel generation:

$$E_t^{act} = \mu^{gas} \cdot F_t^{GT} + \mu^{grid} \cdot P_t^{PIES,b} + \mu^{dies} \sum_{k \in \Omega_{ALL}} \left(P_k^{rated} (1 - s_{k,t}) \right), \tag{4}$$

where E_t^{act} is the total actual system carbon emissions at time t, μ^{gas} is the carbon emission intensity of the GT, and μ^{grid} is the carbon emission intensity of the upstream power grid.

The models for the HX, EB, and cooling equipment are defined as

$$H_t^{HX} = H_t^{HX,in} \cdot \eta^{HX}, \tag{5}$$

$$H_t^{EB} = P_t^{EB} \cdot \eta^{EB}, \tag{6}$$

$$Q_t^{AC} = H_t^{AC,in} \cdot COP^{AC}, \tag{7}$$

$$Q_t^{EC} = P_t^{EC} \cdot COP^{EC}, \tag{8}$$

where H_t^{HX} is the effective thermal power supplied to the heat load by the HX at time t, H_t^{EB} is the effective thermal power output of the EB at time t, Q_t^{AC} is the cooling power output of the AC, and Q_t^{EC} is the cooling power output of the EC at time t.

3.1.3 Energy storage system modeling

The models for the EES and TES devices are

$$E_t^{EES} = E_{t-1}^{EES} \cdot (1 - \sigma^{EES}) + \left(P_t^{EES,c} \cdot \eta^{EES,c} - \frac{P_t^{EES,d}}{\eta^{EES,d}} \right) \cdot \Delta t, \tag{9}$$

$$H_t^{TES} = H_{t-1}^{TES} \cdot (1 - \sigma^{TES}) + \left(H_t^{TES,in} \cdot \eta^{TES,in} - \frac{H_t^{TES,out}}{\eta^{TES,out}} \right) \cdot \Delta t, \tag{10}$$

where E_t^{EES} and E_{t-1}^{EES} denote the energies stored in the EES at times t and $t-1$, respectively. Moreover, $P_t^{EES,c}$ and $P_t^{EES,d}$ are the charging and discharging powers at time t, $\eta^{EES,c}$ and $\eta^{EES,d}$ are the charging and discharging efficiencies, respectively, σ^{EES} is the self-discharge rate of the EES, and H_t^{TES} is the thermal energy stored in the TES at time t.

3.1.4 Multi-region coordinated modeling of shore power load considering allocation flexibility

In view of the heterogeneous characteristics of different operational zones within the port, in this study, we categorize the shore power load into the Pacific Terminal (PT), Cruise Terminal

(CT), and Huisheng Terminal (HS). The parameters of the shore power equipment in each zone are presented in Table 1.

On this energy scheduling strategy, the following assumptions are made:

1. Capacity matching: Differences in individual connection interfaces are disregarded; shore power resources can be flexibly allocated within a terminal zone.
2. Continuous power supply: During a vessel's stay in port, i.e., the interval $\left[t_k^{start}, t_k^{end}\right]$, power must be supplied continuously by either shore power or onboard generation, with no interruptions permitted.
3. Limited switching: Dynamic switching between shore power and onboard generation is permitted to optimize allocation. However, to protect the receiving equipment, the total number of switching events per vessel over the entire process must not exceed two.

Assume that K vessels arrive at the port during the scheduling period T. For each vessel k, the port operator receives the arrival time t_k^{arr} and the estimated departure time t_k^{dep}. To ensure uninterrupted power before departure, the effective power supply window is defined as $\left[t_k^{start}, t_k^{end}\right]$, where $t_k^{start} = t_k^{arr} + 1$ and $t_k^{end} = t_k^{dep} - 1$. The rated power consumption of the vessel is given as P_k^{rated}. A binary variable, $s_{k,t} \in \{0,1\}$, is introduced, where $s_{k,t} = 1$ indicates that vessel k is supplied by SP during interval t, while $s_{k,t} = 0$ denotes supply from onboard generation. The total SP load of PIES at time t is

$$P_t^{shore} = \sum_{k \in \Omega_{ALL}} (P_k^{rated} \cdot s_{k,t}) \quad \forall t \in [1, T]. \tag{11}$$

For each terminal zone, constraints on the number of simultaneous connections and the total capacity must be satisfied:

$$\begin{cases} \sum\limits_{k \in \Omega_m} u_{k,t} \le N_m^{max}, & \forall m \in \{PT, CT, HS\} \\ \sum\limits_{k \in \Omega_m} (P_k^{rated} \cdot s_{k,t}) \le P_m^{max}, & \forall m \in \{PT, CT, HS\} \end{cases} \tag{12}$$

where $u_{k,t}$ is the number of ships connected to shore power during the same time period, Ω_m is the set of vessels berthed at terminal zone m, and N_m^{max} is the upper limit for the number of SP units operating simultaneously.

A binary flexible switching indicator, $y_{k,t} \in \{0,1\}$, is introduced, with switching events represented via differential linearization:

Table 1
Parameters of shore power equipment.

Terminal zone	Number of berths	SP equipment configuration	N_m^{max}	P_m^{max}
PT	6	1 × 3 MW, 2 × 4 MW	3	11 MW
CT	3	2 × 20 MW	2	40 MW
HS	4	2 × 160 kW	2	320 kW

$$\begin{cases} y_{k,t} \geq s_{k,t} - s_{k,t-1}, & \forall t \in \left[t_k^{start} + 1, t_k^{end} \right] \\ y_{k,t} \geq s_{k,t-1} - s_{k,t}, & \forall t \in \left[t_k^{start} + 1, t_k^{end} \right] \\ \sum_{t=t_k^{start}+1}^{t_k^{end}} y_{k,t} \leq 2. & \forall k \in \Omega_{ALL} \end{cases} \tag{13}$$

For periods of resource competition, in this study, we established a flexible allocation mechanism based on the dual attributes of the emission reduction potential and berthing time window. Specifically, these attributes are quantitatively evaluated by calculating the total electricity demand of each vessel during its stay, which is the product of its rated power consumption P_k^{rated} and its effective berthing duration. A larger total electricity demand indicates a higher volume of potential carbon emissions if the vessel relies on onboard diesel generators. Therefore, vessels with a larger total electricity demand are assigned a higher priority for shore power allocation. On the basis of this quantification logic, vessels are classified into three priority levels as follows:

Level 1: Vessels that are already connected and exhibit high emission reduction potential. Switching back to onboard generation is strictly restricted and permitted only under extreme peak shaving requirements.

Level 2: Vessels regarded as flexible loads, which are dynamically dispatched on the basis of emission reduction benefit per unit time. They are guided to switch to onboard generation during resource scarcity or peak electricity price periods, and are prioritized for reconnection when capacity becomes available.

Level 3: Vessels that do not meet the access conditions or whose stay time window is excessively short. These vessels are powered exclusively by onboard generation throughout their stay.

Furthermore, to ensure service fairness and operational feasibility in realistic scenarios involving unexpected berthing delays or simultaneous power requests from multiple vessels, the proposed mechanism operates on a dynamic rolling-horizon update. Whenever a delay or simultaneous request occurs, the system recalculates the priority on the basis of the remaining berthing time. Crucially, the practical feasibility of switching operations is guaranteed by the established switching frequency constraints. Regardless of how fierce the resource competition becomes, the maximum number of switching events is rigidly capped at two per vessel. This hard constraint fundamentally prevents frequent toggling, protecting the onboard electrical equipment from damage while maintaining the equitable distribution of available shore power capacity.

3.2 Upper-level dynamic pricing model

Within the two-level Stackelberg leader–follower game framework, the upper level PESO guides the lower level scheduling by setting the electricity purchase price $\lambda_t^{PIES,b}$ and the sale price $\lambda_t^{PIES,s}$, with the objective of maximizing its own profit.

3.2.1 Objective function

The net profit of PESO, denoted as C^{PESO}, is composed of transaction revenues from the external power market and the internal PIES:

$$\max C^{PESO} = \sum_{t=1}^{T} (\lambda_t^{PESO,s} P_t^{PESO,s} - \lambda_t^{PESO,b} P_t^{PESO,b} + \lambda_t^{PIES,b} P_t^{PIES,b} - \lambda_t^{PIES,s} P_t^{PIES,s}), \quad (14)$$

where $\lambda_t^{PESO,b}$, $\lambda_t^{PESO,s}$, $P_t^{PESO,b}$, and $P_t^{PESO,s}$ represent the transaction prices and quantities between PESO and the external market, whereas $P_t^{PIES,b}$ and $P_t^{PIES,s}$ denote the electricity quantities traded between PIES and PESO.

3.2.2 Constraints

3.2.2.1 Power balance constraint

PESO is required to balance the electricity demand of PIES with the transaction volumes in the external market in real time:

$$\begin{cases} P_t^{PESO,b} - P_t^{PESO,s} = P_t^{PIES,b} - P_t^{PIES,s}, \\ P_t^{PESO,b} \geq 0, \quad P_t^{PESO,s} \geq 0. \end{cases} \quad (15)$$

3.2.2.2 Pricing boundary constraint

To ensure the rationality of electricity pricing transactions, the following constraint is enforced:

$$\lambda_t^{PIES,s} \leq \lambda_t^{PESO,s} \leq \lambda_t^{PESO,b} \leq \lambda_t^{PIES,b}. \quad (16)$$

This constraint ensures the proper transmission of price signals and prevents the occurrence of price inversion.

3.3 Lower-level PIES optimal scheduling model

3.3.1 Objective function

The total operating cost of PIES, denoted as C^{PIES}, comprises energy procurement and sale costs, fuel costs, start up and shut down costs, operation and maintenance costs, carbon trading costs, and penalties related to the clean energy autonomy rate (EAR):

$$\min \mathrm{C}^{PIES} = \sum_{t=1}^{T} (C_t^{PIES,b} - C_t^{PIES,s} + C_t^{fuel} + C_t^{on/off} + C_t^{OM}) + C_t^{carbon} + C_t^{penalty}, \tag{17}$$

where C_t^{OM} denotes the operation and maintenance cost of all PIES equipment during period t, C_t^{carbon} is the total carbon trading cost, and $C_t^{penalty}$ is the total penalty cost for failing to meet the clean energy EAR target.

3.3.2 Constraints

3.3.2.1 Power balance constraints

Electrical power balance:

$$P_t^{GT} + P_t^{OPV} + P_t^{OWT} + P_t^{EES,d} + P_t^{PIES,b} = P_t^{EES,c} + P_t^{baseload} + P_t^{shore} + P_t^{EB} + P_t^{EC} + P_t^{PIES,s}. \tag{18}$$

Thermal energy flow balance:

$$H_t^{GT} = H_t^{AC,in} + H_t^{HX,in}. \tag{19}$$

Heating and cooling power balances:

$$H_t^{HX} + H_t^{EB} + H_t^{TES,out} = H_t^{load} + H_t^{TES,in}, \tag{20}$$

$$Q_t^{AC} + Q_t^{EC} = Q_t^{load}. \tag{21}$$

3.3.2.2 Berth allocation optimization constraints

For any terminal zone $m \in \{PT, CT, HS\}$, the number of connected vessels and the total SP load must satisfy

$$\sum_{k \in \Omega_m} s_{k,t} \le N_m^{max}, \quad \sum_{k \in \Omega_m} (P_k^{rated} \cdot s_{k,t}) \le P_m^{max}. \tag{22}$$

Moreover, the switching frequency of the power supply for a single vessel must adhere to the aforementioned difference linearization constraint to ensure the safety of the vessel's receiving equipment.

3.3.2.3 Energy generation unit constraints

The output power of all conversion equipment is limited by rated capacities. Specifically, the GT must also satisfy ramp rate and status switching constraints:

$$\begin{cases} -R_{down}^{GT} \le P_t^{GT} - P_{t-1}^{GT} \le R_{up}^{GT}, \\ u_t^{GT} + v_t^{GT} \le 1, \end{cases} \tag{23}$$

where R_{down}^{GT} and R_{up}^{GT} are the ramp rate limits, and u_t^{GT} and v_t^{GT} are logic variables for unit start-stop.

3.3.2.4 Renewable energy output constraints

$$\begin{cases} 0 \le P_t^{OPV} \le P_t^{OPV,max} \\ 0 \le P_t^{OWT} \le P_t^{OWT,max} \end{cases} \tag{24}$$

Here, $P_t^{OPV,max}$ and $P_t^{OWT,max}$ denote the upper bounds for offshore photovoltaic and OWT generation during interval t, respectively.

3.3.2.5 Electricity trading boundary constraints

$$\begin{cases} 0 \le P_t^{PIES,b} \le P^{b,max} \\ 0 \le P_t^{PIES,s} \le P^{s,max} \end{cases} \tag{25}$$

Here, $P^{b,max}$ and $P^{s,max}$ represent the upper limits for electricity purchased and sold by PIES, respectively.

3.3.2.6 Energy storage system constraints

Electrical and TES equipment must satisfy charging and discharging efficiency requirements, capacity limits, and state-of-energy balance between the start and end of the scheduling period:

$$\begin{cases} E_t^{EES,min} \le E_t^{EES} \le E_t^{EES,max}, \\ E_0^{EES} = E_T^{EES}, \\ \eta^{EES,c} + \eta^{EES,d} \le 1, \end{cases} \tag{26}$$

$$\begin{cases} H_t^{TES,min} \le H_t^{TES} \le H_t^{TES,max}, \\ H_0^{TES} = H_T^{TES}, \\ \eta^{TES,in} + \eta^{TES,out} \le 1, \end{cases} \tag{27}$$

where $E_t^{EES,min}$, $E_t^{EES,max}$, $H_t^{TES,min}$ and $H_t^{TES,max}$ are the minimum and maximum capacity limits for EES and TES, respectively.

3.4 Evaluation indicators

To assess the performance of the proposed scheduling strategy in terms of environmental protection, energy autonomy, and service quality, the following key indicators are defined as follows.

3.4.1 Carbon emission reduction

The total CO_2 emissions avoided, which result from the consumption of clean energy and the substitution effect of shore power, are quantified as

$$Q^{CO2,red} = \sum_{t=1}^{T} \left[P_t^{ren,con} \cdot \mu_{\text{grid}} + P_t^{shore} \cdot (\mu_{diesel} - \mu_{grid}) \right], \tag{28}$$

where μ_{grid} and μ_{diesel} are the carbon emission factors for the power grid and ship diesel engines, respectively, and $\mu_{diesel} - \mu_{grid}$ represents the net reduction effect of SP substitution.

3.4.2 Clean EAR

EAR reflects the degree of port energy self-sufficiency and is defined as the proportion of locally consumed renewable energy relative to the total electricity consumption:

$$R^{EAR} = \frac{\sum_{t=1}^{T} \left(P_t^{OPV} + P_t^{OWT} \right)}{\sum_{t=1}^{T} \left(P_t^{baseload} + P_t^{shore} + P_t^{EB} + P_t^{EC} + P_t^{EES,c} \right)} \times 100\%. \tag{29}$$

3.4.3 Shore power service satisfaction (SPSS)

SPSS measures service quality from the perspective of the user and is defined as the ratio of the actual SP energy supplied to the total electricity demand of the vessels:

$$P^{SPSS} = \frac{\sum_{k\in\Omega_{ALL}} \sum_{t=t_k^{arr}}^{t_k^{dep}} \left(P_k^{rated} \cdot s_{k,t} \cdot \Delta t\right)}{\sum_{k\in\Omega_{ALL}} E_k^{req}} \times 100\%, \tag{30}$$

where E_k^{req} is the total electricity demand of vessel k during its berthing.

3.4.4 Vessel fairness indicators

To quantitatively evaluate the service fairness among individual vessels and address potential conflicts of user interests, the individual SPSS for each vessel k is defined as

$$P_k^{ISPSS} = \frac{\sum_{t=t_k^{arr}}^{t_k^{dep}} \left(s_{k,t} \cdot \Delta t\right)}{t_k^{dep} - t_k^{arr}} \times 100\%. \tag{31}$$

On the basis of the individual satisfaction of each vessel, Jain's fairness index (FI) is newly introduced to measure the overall equity of resource allocation across the entire port:

$$FI = \frac{\left(\sum_{k\in\Omega_{ALL}} P_k^{ISPSS}\right)^2}{\Omega_{ALL} \cdot \sum_{k\in\Omega_{ALL}} \left(P_k^{ISPSS}\right)^2}, \tag{32}$$

where a higher FI value indicates a more equitable allocation of shore power resources among competing vessels.

4. Case Analysis

To validate the effectiveness of the proposed optimal scheduling model using the Stackelberg leader–follower game algorithm, in this study, we select the PT, HS, and CT of a port in northern China as the simulation objects. The scheduling horizon is set to 24 h, with a time step of 1 h.

PIES integrates OWT, OPV, GT, and various energy storage devices. The rated installed capacity of OWT is set to 38 MW and that of OPV is set to 26 MW. The output data of these renewable sources are collected using the ultrasonic wind and shortwave radiation sensors deployed within the port area. To quantitatively evaluate the forecasting stability enabled by these high-resolution sensor settings, the mean absolute percentage error (*MAPE*) of the predicted output generation is calculated. Supported by the 15-min aggregated sensing matrix, *MAPE* is strictly restricted to 4.32% for OWT and 5.11% for OPV. This notably low forecast error range proves the robustness of the data acquisition layout and guarantees a highly stable

deterministic input boundary for the day-ahead economic scheduling of PIES. The operational parameters of the GT and energy storage systems, including ramp rate constraints and operation coefficients, are configured in accordance with technical specifications. On the load side, typical day data for the winter season are adopted. The vessel arrival and departure schedules, generated from port operation logs, encompass the three representative terminal zones. The berthing schedules for the CT, PT, and HS are summarized in Table 2, encompassing the rated power consumption, estimated arrival times, and estimated departure times for all vessels within the three terminal zones. During the scheduling horizon, 7 vessels are berthed at the CT, whilst the PT and HS accommodate 16 and 11 vessels, respectively.

The renewable energy generation profiles are shown in Fig. 2(a), and the time-of-use electricity and gas prices are shown in Fig. 2(b).

Table 2
Berthing schedules for CT, PT, and HS zones.

CT				PT				HS			
Number	P_k^{rated}	t_k^{arr}	t_k^{dep}	Number	P_k^{rated}	t_k^{arr}	t_k^{dep}	Number	P_k^{rated}	t_k^{arr}	t_k^{dep}
S-1	3000	1	11	S-8	2500	1	9	S-24	120	1	7
S-2	7600	6	18	S-9	3550	2	11	S-25	150	2	9
S-3	16200	11	17	S-10	2100	4	10	S-26	90	1	11
S-4	14500	14	22	S-11	2350	1	8	S-27	110	10	15
S-5	8000	3	10	S-12	3800	2	12	S-28	140	12	18
S-6	12000	18	24	S-13	3900	9	16	S-29	130	11	18
S-7	18000	20	24	S-14	2600	11	17	S-30	100	20	24
—	—	—	—	S-15	2750	15	24	S-31	155	6	14
—	—	—	—	S-16	2900	18	23	S-32	120	15	22
—	—	—	—	S-17	3050	21	24	S-33	145	14	20
—	—	—	—	S-18	3100	9	19	S-34	115	19	24
—	—	—	—	S-19	3250	16	24		—	—	—
—	—	—	—	S-20	2800	5	12		—	—	—
—	—	—	—	S-21	3400	13	19		—	—	—
—	—	—	—	S-22	2200	18	24		—	—	—
—	—	—	—	S-23	3600	20	24		—	—	—

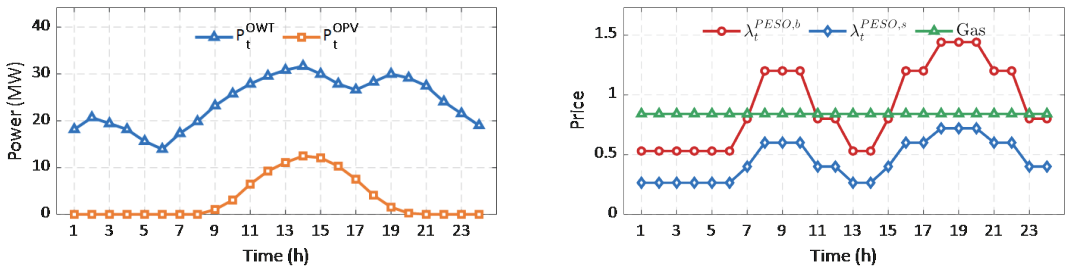

(a) (b)

Fig. 2. (Color online) Basic operational parameters of the system. (a) Renewable energy generation profiles and (b) time-of-use electricity and gas prices.

To comprehensively evaluate the advantages of the two-level game mechanism and the flexible shore power scheduling strategy in terms of economic efficiency, environmental performance, and service quality, the following two optimization strategies are established for in-depth analysis:

Strategy 1: Baseline strategy. PESO does not formulate dynamic electricity prices for PIES. Instead, the electricity market price is directly applied as the purchase and sale price for PIES. The connection of vessels to shore power is not optimized; the timing of shore power supply is determined solely by the vessel arrival sequence.

Strategy 2: Proposed strategy. This strategy simultaneously considers the Stackelberg leader–follower game and flexible shore power allocation. Building upon the two-level game framework, this scenario fully exploits the response potential of vessel loads in both temporal and spatial dimensions. Through a multi-region coordinated flexible shore power allocation mechanism, the matching outcome between energy supply and flexibility demand is demonstrated as follows.

4.1 Electricity prices under different strategies

On the basis of two scheduling strategies, the purchase price of electricity from the power market for PESO and that for PIES from PESO in Strategy 1, as shown in Fig. 3, are represented by the grey dashed line, while the sale price is indicated by the grey dotted line. The red solid line denotes the purchase price of electricity for PIES from PESO, and the blue solid line denotes the sale price, where the purchase and sale prices between PESO and the power market remain identical. In Strategy 2, PESO can secure a reasonable profit margin through the dynamic purchase-sale price differential, as illustrated by the red and blue solid lines in Fig. 3, whilst simultaneously guiding the optimal dispatch of PIES. This pricing mechanism, based on the Stackelberg game, utilizes temporal fluctuations in price signals to guide shore power loads for peak shaving and valley filling, thus achieving a win–win outcome without modifying external electricity prices.

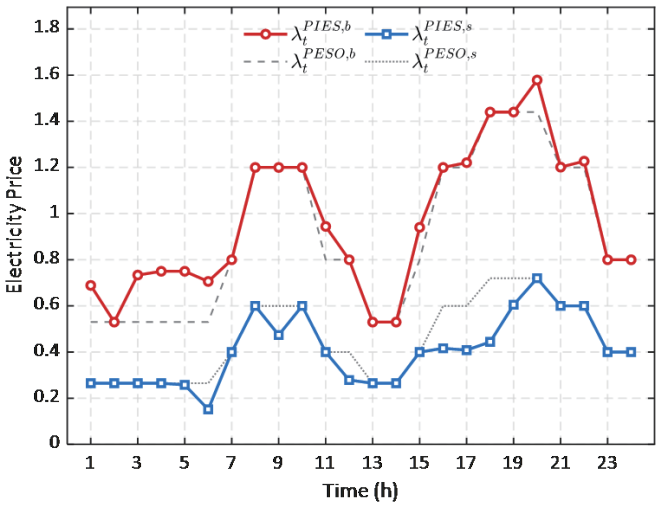

Fig. 3. (Color online) Transaction price.

4.2 Vessel berthing decisions under flexible shore power allocation

The total load demand under Strategy 1 is shown in Fig. 4. It indicates that high power is demanded during the peak electricity price interval from 07:00 to 11:00. By contrast, based on the Stackelberg game and flexible shore power allocation using Strategy 2, the shore power load exhibits significant sensitivity to price signals, as shown in Fig. 5. Substantial peak shaving and valley filling are thus achieved by actively shifting demand from high-price periods to the low-price interval between 11:00 and 15:00. Therefore, the power supply pressure can be mitigated during peak demand periods while considerably reducing the total operating costs of the port.

The shore power charging decisions before and after the implementation of flexible shore power allocation are illustrated in Figs. 6 and 7, respectively. The results reveal that the total shore power load demand curve in the port is primarily attributable to the rescheduling of shore power supply time intervals for specific vessels. These include vessels S-1 and S-2 at CT, vessels S-9, S-11, S-16, S-17, S-20, S-21, and S-23 at PT, and vessels S-24, S-25, S-26, S-27, S-29, and S-32 at HS.

Figure 6(a) illustrates the scheduling at the CT under Strategy 1. It demonstrates that vessel S-2 is unable to access shore power using the FCFS approach, relying solely on onboard diesel generators instead. In the corresponding Strategy 2, as shown in Fig. 7(a), the power supply sequence is actively adjusted through a flexible allocation mechanism. The shore power supply to S-1 is terminated prematurely to reallocate the resource quota to S-2, thus exhibiting higher emission reduction potential. Figure 6(b) reflects the issue of uneven resource occupancy at the PT under the conventional strategy, where S-8 occupies a limited shore power berth. Figure 7(b) exhibits the dynamic optimal scheduling for vessels such as S-9, S-11, S-18, and S-21. However, for vessels such as S-17, the power is supplied exclusively by onboard generators owing to an ineffective berthing window to accommodate the minimum time required for equipment connection and response adjustment. Through this filtering mechanism, shore power interfaces are reserved for vessel S-23, thereby enhancing the overall SPSS.

Figure 6(c) shows that adhering to the FCFS strategy prevents critical loads such as S-26, S-29, and S-32 from utilizing shore power. Strategy 2, as shown in Fig. 7(c), fully accounts for equipment capacity limits and vessel priorities, vacating necessary power capacity for S-26, S-29, and S-32 through the flexible scheduling of smaller loads such as S-24 and S-27. It implies

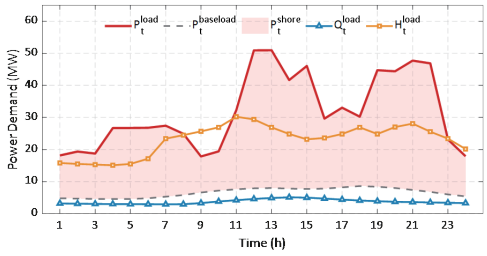

Fig. 4. (Color online) Total power, heating, and cooling demand in Strategy 1.

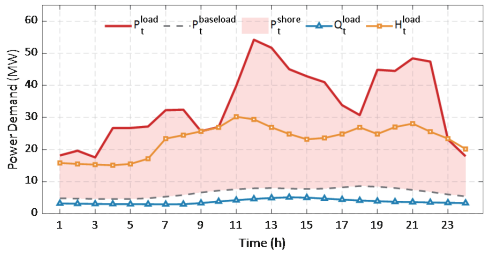

Fig. 5. (Color online) Total power, heating, and cooling demand in Strategy 2.

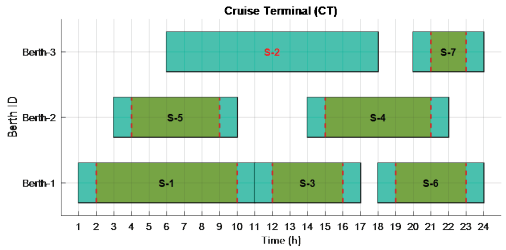

(a)

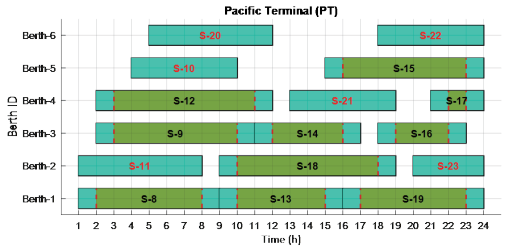

(b)

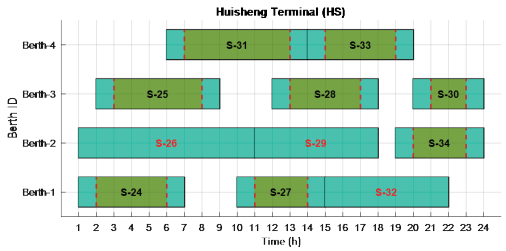

(c)

Fig. 6. (Color online) Shore power scheduling decisions in Strategy 1. (a) CT, (b) PT, and (c) HT.

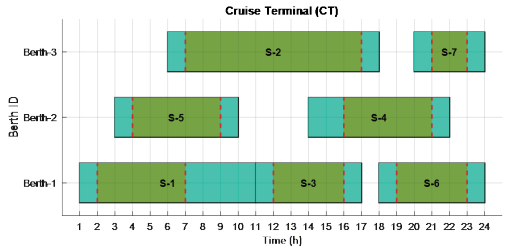

(a)

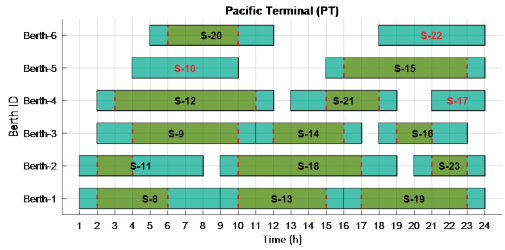

(b)

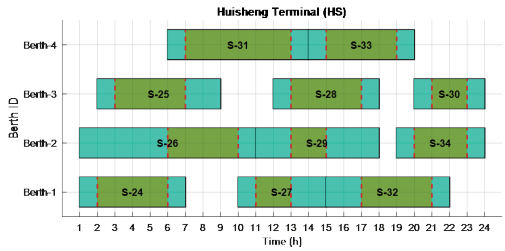

(c)

Fig. 7. (Color online) Shore power scheduling decisions in Strategy 2. (a) CT, (b) PT, and (c) HT.

that this flexible allocation under multi-region coordination effectively overcomes resource mismatching with traditional fixed allocation models, thus achieving precise matching between energy supply and vessel flexibility demand.

4.3 PIES equipment operation

The power supply balance under Strategy 1 is shown in Fig. 8, where the shore power load P_t^{shore} behaves as a rigid load. It has intensive power demand during peak market price intervals such as 09:00 to 11:00. The electrical power balance results using flexible shore power allocation are presented in Fig. 9. As observed from this figure, both the electrical load and the various power devices can respond to the scheduling signals driven by the electricity price. During high price periods, such as 09:00, the power supply decision of PIES tends to reduce the shore power supply to vessels, thereby lowering the total electrical load. Conversely, during low price

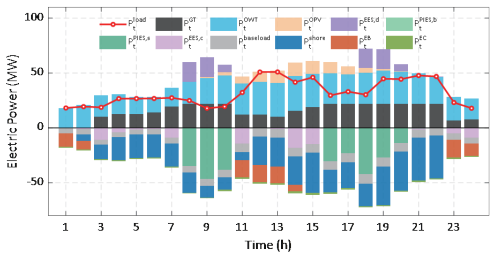

Fig. 8. (Color online) Power supply balancing for PIES in Strategy 1.

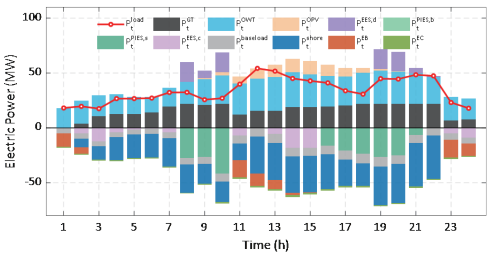

Fig. 9. (Color online) Power supply balancing for PIES in Strategy 2.

periods, such as 13:00 to 14:00, PIES preferentially charges the energy storage systems and shifts the shore power supply, thus reducing PIES operating costs and improving SPSS.

As illustrated in Figs. 10 and 11, Strategy 1 follows a rigid logic where multi-energy flows are insensitive to price signals. Conversely, Strategy 2 leverages the Stackelberg game for optimal coupled scheduling. Under dynamic pricing, the system increases EB output during the 12:00 to 14:00 electricity price trough to store low-cost heat in the TES for peak periods. Moreover, during electricity price peaks, the HX provides more waste heat to drive AC refrigeration, minimizing EC power consumption and successfully optimizing both energy costs and operational efficiency.

4.4 Comparison of evaluation indicators and economic indicators

4.4.1 Comparison of evaluation indicators

As shown in Table 3, the proposed Strategy 2 elevates CO_2 reduction to 459.35 tons and the clean EAR to 76.48%. By prioritizing vessels with high emission demands and long stays such asS-2, this mechanism avoids the resource mismatch of the traditional arrival-sequence method. Consequently, the overall SPSS scales to 88.30% without extra investment, optimizing economic and environmental indicators synergistically.

4.4.2 Comparison of economic indicators

Table 4 presents the net profit of PESO and the total operating cost of PIES under the two distinct scheduling strategies. The profit of PESO is derived from the price differential of electricity purchased by PIES from PESO. In Strategy 1, the purchase and sale prices for PIES are identical to those in the electricity market; consequently, PESO accrues no net profit.

In comparison with Strategy 1, the profit of PESO under Strategy 2 rises from zero to 2917 US$. This is not achieved by merely extracting surplus from PIES, but rather through the redistribution of benefits and flexibility premiums arising from the Stackelberg leader–follower game. Concurrently, the operating cost of PIES is reduced by 5960US$, corresponding to a

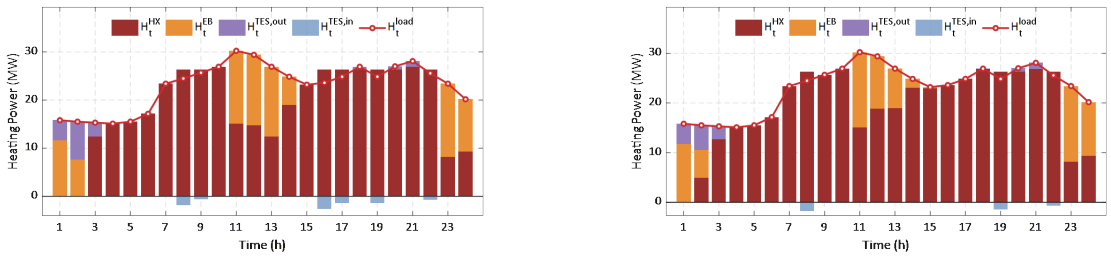

(a) (b)

Fig. 10. (Color online) Heating supply balancing for PIES. (a) Strategy 1 and (b) Strategy 2.

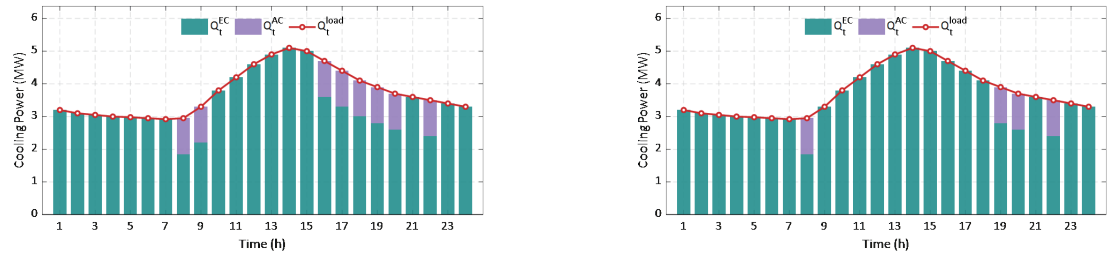

(a) (b)

Fig. 11. (Color online) Cooling supply balancing for PIES. (a) Strategy 1 and (b) Strategy 2.

Table 3
Statistical table of evaluation indicators.

	Carbon emission reduction (total CO_2)	Clean EAR (%)	SPSS (%)
Strategy 1	438.64	72.07	77.18
Strategy 2	459.35	76.48	88.30

Table 4
Statistical table of economic indicators.

	PIES min.operating cost ($)	PESO max. net profit ($)
Strategy 1	40130	—
Strategy 2	34170	2917

reduction of 14.85%. The significant decline in PIES costs is largely attributable to the flexible shore power allocation mechanism. By shifting vessel shore power demand from high electricity price periods to low price periods, the system secures substantial savings in electricity procurement expenditure. Moreover, Strategy 2 fully leverages the coupled regulation capabilities of the GT and the thermal and EES devices. Through thermal and EES during low price periods, the system effectively curtails energy procurement volumes during high price periods, thereby realizing global economic optimality for the electricity, heating, and cooling multiple-energy system. Through the deep coupling of dynamic price signals and flexible shore

power allocation, Strategy 2 successfully overcomes the zero-sum game deadlock in conventional fixed pricing models, thereby achieving a win–win outcome.

4.5 Sensitivity analysis of PIES cost and PESO profit

The Stackelberg game assumes perfect information symmetry between PESO and PIES, utilizes linear cost functions for tractability, and relies on the rational price elasticity of shore power loads to shift demand.

To explicitly evaluate parameter sensitivity, Table 5 illustrates the impact of natural gas fuel and grid electricity price variations ranging from −20 to +20% on system outcomes. While absolute financial metrics logically scale with input prices, as demonstrated by a 20% grid price surge that pushes PIES costs to 36859 US$ and PESO profits to 3210 US$, the game consistently converges to a stable equilibrium. Crucially, across all extreme market volatility scenarios, PIES rigorously maintains substantial cost savings compared with the baseline rigid strategy of 40130 US$, confirming the structural robustness of the proposed dispatch decisions.

4.6 Comprehensive robustness and individual fairness analysis

Table 6 clearly illustrates the drawbacks of the conventional Strategy 1. This scheme creates severe resource imbalance: it completely meets the requirement of S-1 but allocates no resources to late requests S-2 and S-32. Our proposed Strategy 2 addresses this issue via dynamic resource redistribution. By lowering S-1's satisfaction level to 63%, we can fully satisfy S-2 and achieve 80% satisfaction for S-32, lifting the Jain fairness index from 0.74 to 0.88.

Table 5
Sensitivity analysis of PIES cost and PESO profit.

Variation	Natural gas price		Grid electricity price	
	PESO profit ($)	PIEScost ($)	PESO profit ($)	PIEScost ($)
−20%	2846	32257	2652	31845
−10%	2873	33216	2780	32981
0%	2917	34170	2917	34170
+10%	2965	35189	3065	35428
+20%	3020	36242	3210	36859

Table 6
Comprehensive evaluation of individual fairness and system robustness under diverse scenarios.

Evaluation scope	Metrics	Strategy 1	Strategy 2	Summer	High vessel density	Low renewable output
Individual vessel	S-1 ISPSS	100%	63%	63%	50%	63%
	S-2 ISPSS	0%	100%	80%	60%	70%
	S-32 ISPSS	0%	80%	80%	60%	80%
System-wide vessels	FI	0.74	0.88	0.85	0.81	0.84
	PIES operating cost ($)	40130	34170	32215	38408	37153

Extensive multi-scenario tests verify the strong robustness of the model. Even under harsh operating conditions with tight capacity, such as dense vessel arrivals and weak renewable power supply, no demand is fully rejected, and the system-wide fairness index is sustained above 0.81. Owing to ample renewable energy in the summer load case, the operating cost drops to 32215 US$. Compared with the fixed baseline strategy costing 40130 US$, our scheduling method reduces expenses significantly across all test scenarios, proving its capability to balance system economic performance and allocation fairness effectively.

5. Conclusions

In this study, a shore power priority scheduling model for a port virtual power plant has successfully achieved a flexible power supply switching between shore power and onboard generators. The computational results demonstrate that PESO can attain an average daily profit of US$ 2917, whilst the operating cost of PIES is reduced by 14.85%. Concurrently, a carbon dioxide emission reduction reaches 459.35 tons, and SPSS improves from 77.18 to 88.30%. The findings verify that the deep integration of physical-sensor-based perception with an intelligent game theoretic scheduling strategy can enhance the port energy utilization efficiency so that green shipping can be promoted effectively. Furthermore, while the absolute values of CO_2 reduction are tied to the specific port scale, the relative operational benefits, such as the 14.85% cost reduction, demonstrate strong scalability to larger seaports with similar microgrids. Regarding policy implications, carbon pricing and targeted shore power subsidies emerge as the most significant drivers. A higher carbon tax or favorable tariff design would substantially expand the flexibility premium for PIES, incentivizing more vessels to participate in dynamic scheduling. In future work, we will further investigate uncertainties in multi-source sensor data fusion, including fluctuations in vessel arrival timing and dynamic risks in electricity markets, with the aim of constructing a more robust framework for port energy intelligent sensing and optimal scheduling.

Acknowledgments

This work was supported by the Tianjin Carbon Peak and Carbon Neutrality Technology Major Project (Project No. 24ZXTKSN00030) and the S&T Program of Hebei (Project No. 24464401D).

References

1 M. A. Dulebenets: Swarm Evol. Comput. **80** (2023) 101334. https://doi.org/10.1016/j.swevo.2023.101334
2 B. K. Li, P. Afkhami, R. Khayamim, M. Borowska-Stefanska, S. Wisniewski, A. M. Fathollahi-Fard, S. Ozkul, and M. A. Dulebenets: Transp. Res. Part E-Logist. Transp. Rev. **198** (2025) 104104. https://doi.org/10.1016/j.tre.2025.104104
3 A. Molavi, G. J. Lim, and J. Shi: Appl. Energy **272** (2020) 115188. https://doi.org/10.1016/j.apenergy.2020.115188
4 L. Y. Ran, B. N. Liu, G. Q. Zhang, and Y. X. Cheng: Expert Syst. Appl. **269** (2025) 126406. https://doi.org/10.1016/j.eswa.2025.126406
5 B. P. Kumar, D. S. Pillai, N. Rajasekar, M. Chakkarapani, and G. S. Ilango: IEEE Trans. Ind. Electron. **68** (2021) 5921. https://doi.org/10.1109/TIE.2020.2998750

6 N. Kumar, B. Singh, and B. K. Panigrahi: IEEE Trans. Transp. Electrif. **9** (2023) 2583. https://doi.org/10.1109/TTE.2022.3213253
7 X. Xu, X. Bai, J. Wang, Y. Lu, L. Li, W. Lu, and Z. Li: J. Chang'An University. Natural Sci. Edition **45** (2025) 140. https://doi.org/10.19721/j.cnki.1671-8879.2025.05.012
8 A. Imai, E. Nishimura, and S. Papadimitriou: Transp. Res. Part B-Methodological **39** (2005) 197. https://doi.org/10.1016/j.trb.2004.03.004
9 T. P. V. Zis: Transp. Res. Part A-Policy Pract. **119** (2019) 82. https://doi.org/10.1016/j.tra.2018.11.003
10 Y. Wang and T. Y. Zou: J. Marine Sci. Eng. **12** (2024) 684. https://doi.org/10.3390/jmse12040684
11 A. Molavi, J. Shi, Y. Wu, and G. J. Lim: Appl. Energy **258** (2020) 114022. https://doi.org/10.1016/j.apenergy.2019.114022
12 Y. P. Li, X. H. Cao, and Z. J. Li: J. Energy Storage **125** (2025) 116807. https://doi.org/10.1016/j.est.2025.116807
13 Ç. Iris and J. S. L. Lam: Renewable Sustainable Energy Rev. **112** (2019) 170. https://doi.org/10.1016/j.rser.2019.04.069
14 C. Xiong, Y. Su, H. Wang, Z. Dong, M. Tian, and B. Shi: Appl. Energy **373** (2024) 123948. https://doi.org/10.1016/j.apenergy.2024.123948
15 I. Sarantakos, S. Nikkhah, M. Peker, A. Bowkett, T. Sayfutdinov, A. Alahyari, C. Patsios, J. Mangan, A. Allahham, E. Bougioukou, A. Murphy, and K. Pazouki: Cleaner Logist. Supply Chain **10** (2024) 100144. https://doi.org/10.1016/j.clscn.2024.100144
16 A. N. Lin, S. L. Wen, M. Zhu, and Y. Xu: IEEE Trans. Intell. Veh. **9** (2024) 3558. https://doi.org/10.1109/tiv.2024.3351607
17 S. L. Wen, Z. X. Dong, T. Y. Zhao, M. Zhu, and Y. Q. Huang: Energy **313** (2024) 133748. https://doi.org/10.1016/j.energy.2024.133748
18 Y. Z. Zhou, Y. Li, W. T. Huang, S. Chen, H. X. Zang, and N. L. Tai: Appl. Energy **400** (2025) 126598. https://doi.org/10.1016/j.apenergy.2025.126598
19 W. N. Zhao, K. Ma, Z. W. Qu, S. L. Guo, F. J. Qi, and W. C. Sun: Electric Power Syst. Res. **244** (2025) 111527. https://doi.org/10.1016/j.epsr.2025.111527
20 J. Pan, W. Jiang, H. Zhu, S. Jiang, F. Chen, X. Wang, and H. Huang: Sustainable Energy Res. **12** (2025) 61. https://doi.org/10.1186/s40807-025-00213-8
21 Y. T. Sun, Y. J. Guo, Q. Zhang, and Y. W. Jia: Energy **322** (2025) 135640. https://doi.org/10.1016/j.energy.2025.135640
22 Z. F. Liu, Y. Y. Liu, H. J. Jia, X. L. Jin, T. H. Liu, and Y. Z. Wu: Appl. Energy **390** (2025) 125868. https://doi.org/10.1016/j.apenergy.2025.125868
23 T. R. Zhang, W. B. Zhao, Q. F. He, and J. N. Xu: Sustainability **17** (2025) 648. https://doi.org/10.3390/su17020648